Comparison between cooling strategies for power electronic devices: fractal mini-channels and arrays of impinging submerged jets

IOP Conf. Series: Journal of Physics: Conf. Series **1224** (2019) 012014 doi:10.1088/1742-6596/1224/1/012014

Comparison between cooling strategies for power electronic devices: fractal mini-channels and arrays of impinging submerged jets

N Baraldi[1], A Fregni[1], M Sabato[1], E Stalio[1], F Brusiani[2], M Tranchero[2] and T Baritaud[2]

[1] Dipartimento di Ingegneria "Enzo Ferrari", Università di Modena e Reggio Emilia
[2] Ferrari S.p.A.

E-mail: enrico.stalio@unimore.it

Abstract. Power electronic devices like Insulated Gate Bipolar Transistors (IGBTs) and diodes are often characterized by power densities and dimensions that could result in very high heat flux densities. In order to guarantee the expected performance and lifetime for these components, dedicated active cooling devices are usually adopted. In the present paper, the comparison between two different cooling strategies for power electronics is presented: fractal-channel design and submerged impinging jets. Each cooling strategy is tested on two different geometrical configurations. Water is used as coolant in all cases. Assessment of the considered cooling methods is done through application of the selected configuration in a simplified system composed by a rectangular chip (heat source) separated from the coolant by a solid block.

Three-dimensional conjugated heat transfer simulations are performed by using RANS solver implemented in OpenFOAM and two-equations turbulence models, resolving also the viscous sublayer. Numerical results allow to compare the cooling strategies in terms of maximum chip temperature, overall chip-to-coolant thermal resistance, and pumping power required. In summary, the fractal-channel design shows limitations in guaranteeing low chip temperatures at an affordable pumping power. The submerged impinging jets approach shows very high local heat transfer coefficient by which it is possible to tailor the cooling effect on specific hot spots.

Nomenclature

Greek Symbols

δ	Nozzle height $[m]$
η , ψ	Numerical coefficients for fractal-channel geometries
Γ	Ratio between height and width of a fractal-channel branch
γ	Ratio between hydraulic diameters of two consecutive branches
ρ	Fluid density $[kg/m^3]$
θ	Ratio between lengths of two consecutive branches
ζ, α, β	Dimensionless coefficients in Nusselt number correlation

Roman Symbols

A	Chip plan area $[m^2]$
AR	Aspect ratio
c	Specific heat $[J/(kgK)]$
c_D	Discharge coefficient
C_{k+1}	Ratio of heat transfer rate between two consecutive branches in fractal channels
D	Nozzle diameter $[m]$
d	Dimensionless hydraulic diameter of a fractal-channel branch
H	Dimensionless height of a fractal-channel branch
h	Heat transfer coefficient $[W/(m^2K)]$
L	Dimensionless length of a fractal-channel branch
l	Length $[m]$
M	Wet surface per unit length of a fractal-channel branch $[m]$
m	Mass $[kg]$
N	Number of nozzle
n	Number of bifurcations in fractal channels
Nu	Nusselt number
P	Power $[W]$
p	Static pressure $[Pa]$
P_g	Heat generation rate of the chip $[W]$
P_p	Pumping power $[W]$
Pr	Prandtl number
Q	Heat $[J]$
R_{th}	Thermal resistance $[K/W]$
Re	Reynolds number
S	Inlet-section area $[m^2]$
T	Temperature $[K]$
u	Velocity $[m/s]$
V	Fluid volume $[m^3]$
W	Dimensionless width of a fractal-channel branch
y^+	Dimensionless wall distance
Z	Jet-to-target spacing $[m]$

Subscripts, superscripts and other symbols

0	Relative to the first fractal-channel branch
$1, 2$	Sides of the chip in plan view
$\bar{}$	Surface averaged
$\dot{}$	Per unit time
b	Bulk condition
id	Ideal
in	Inlet
max	Maximum
out	Outlet
r	Real
ref	Reference condition
w	At liquid-solid interface

1. Introduction

Heat removal from power electronic devices is a technical problem common to many industrial fields, including the recent application of power electronics to hybrid traction systems. This study investigates and compares two single-phase liquid cooling devices for a single chip: the first one employs a network of fractal channels while the second one uses an array of submerged impinging jets. The efficiency of each cooling strategy is investigated on two test benches: a baseline configuration and an improved configuration designed to improve the baseline thermal and fluid-dynamics performance.

Application of fractal channels is considered a promising solution for the cooling of power electronics thanks to the large heat transfer surface involved. In Ref. [1], it is demonstrated that a tree-shaped structure increases its heat transfer capabilities and decreases its pumping power request for larger number of fractal levels. In Ref. [2], fractal channels are compared against serpentine channel. Results show the improvements of tree-shaped structures in heat transfer efficiency and pressure drop reduction. In Ref. [3], tree-shaped nets on a square chip are investigated and compared to straight and serpentine networks also. Results show that at the cost of a moderate increment in pressure drop, the temperature of the chip decreases for large numbers of branching levels. Also Escher and coworkers [4] compare fractal channels against a parallel channel cooler. In their study, parallel channels having a constant cross section show better cooling efficiency than fractal ones. From this brief literature survey, it appears clearly that tree-shaped channels have a good potential but their performance can depend strongly on the specific application. In the present paper the crucial importance of the ratio between wet surface and heat transfer area in tree-shaped channels is discussed.

A different technique for the cooling of power electronics is the use of two-phase or single-phase arrays of impinging jets. By this technique, it is possible to guarantee a high cooling efficiency on specific hot spots at an affordable pumping power request. Jörg *et al.* [5] clearly showed as the individual cooling of semiconductors, for example by micro-jets, offers new perspectives in the design of power electronic modules. As showed in [6], in general, with respect to the single jet the use of jet arrays is a preferred cooling configuration because of the higher area-averaged heat transfer coefficient reached for a specific coolant flow rate. As for the fractal cooling approach, also for the impinging jet method there are possible drawbacks due to the larger non uniformity in chip surface temperature and cooling efficiency sensitiveness to the manufacturing tolerances [7].

In the present paper, the application of the tree-shaped fractal channels and of the impinging jet arrays in cooling electronic devices have been evaluated by performing 3D-CFD conjugated

simulations. The adopted numerical procedure is validated against experimental data and results are compared and discussed from both heat transfer coefficients and pumping power requirement point of views. Heat generation rate of the chip and inlet temperature of the coolant are the same for all the simulated configurations, although simulations on the fractal channels are carried out for imposed volumetric flow rate of the coolant while submerged jets are computed under a given pressure drop, this is done in view of numerical considerations and the two cases represent the same practical problem, very close to electric traction applications.

2. Method of analysis

Results reported in the present paper are obtained by simulation and using the open source code OpenFOAM (www.openfoam.com). The specific solver employed is the *chtMultiRegionSimpleFoam*, a steady-state solver which imposes mass conservation through the SIMPLE algorithm and allows for the inclusion of conduction heat transfer in solid walls, thus being able to calculate conjugate heat transfer cases. As the Reynolds number in the heat transfer passages investigated is *transitional* in most of the cases considered here, a RANS method is employed, using a $k-\omega$ SST turbulence model [8] for the submerged impinging jets case and a $k-\varepsilon$ model for the fractal channels, see for example [9]. For low turbulence levels these models calculate a very small eddy diffusivity and provide a total viscosity term which is very close to the coolant molecular viscosity. Spatial discretisation is done by a second order central scheme for the diffusive term and by a first order upwind scheme for advection.

Given the linear temperature field behaviour, the mesh in the solid region requires in general a smaller number of cells with respect to the fluid regions. As a consequence of that, a non-conformal mesh interface is present at solid-fluid interface in the fractal channels simulations, while for the impinging jet cases a conformal mesh is adopted. The mesh is in general very fine both for the fractal channels and the submerged impinging jets, with a maximum distance from the wall (y^+) always lower than 4. The average y^+ value is below 1 in each simulation, therefore a low-Reynolds approach is followed and the flow field is directly calculated also in wall proximity. Further hypotheses considered in the present study are: viscous dissipation is negligible, the Knudsen number is very small, and buoyancy effects are negligible. All of them have been checked by a preliminary analysis.

Performance of the different cooling strategies have been assessed using the following criteria

- Maximum chip temperature T_{max},
- overall heat transfer coefficient,
- thermal resistance,
- pumping power.

The overall heat transfer coefficient $\overline{h}$ is defined as:

$$\overline{h} \equiv \frac{\dot{Q}}{A_w \left(\overline{T}_w - T_{b,in}\right)} \tag{1}$$

where $\dot{Q}$ is the heat transferred from the chip to the liquid coolant in the time unit, A_w is the liquid-solid interface areas, $\overline{T}_w$ is the average temperature of this interface and $T_{b,in}$ is the bulk temperature at the inlet.

The thermal resistance R_{th} between chip and coolant is defined similarly

$$R_{th} = \frac{T_{max} - T_{b,in}}{\dot{Q}} \tag{2}$$

see also Ref. [10].

The mechanical energy per time unit for maintaining an assigned flow rate is calculated as

$$P_p = \dot{V}\Delta p \tag{3}$$

where $\dot{V}$ is the volumetric flow rate and Δp is the static pressure drop between the inlet and the outlet sections, $\Delta p = p_{in} - p_{out}$.

To preserve confidentiality of configurations and conditions, data are presented in a non-dimensional form using reference quantities defined as follows. The reference length is

$$l_{\text{ref}} = \sqrt{l_1 l_2} \tag{4}$$

where $l_1 l_2 = A$ is the chip plan area. The reference velocity definition is based upon the bulk velocity at the inlet or the imposed pressure drop, depending on the specific case considered:

- for imposed pressure drop (impinging jet cases)

$$u_{\text{ref}} = \sqrt{\frac{2\,\Delta p}{\rho}} \tag{5}$$

- for given volumetric flow rate (fractal channels)

$$u_{\text{ref}} = u_b = \frac{\dot{V}}{S} \tag{6}$$

where $\dot{V}$ is the volumetric flow rate and S is the inlet-section area. The reference temperature is

$$T_{\text{ref}} = \frac{P_g}{\rho u_{\text{ref}}\, c\, S} \tag{7}$$

where P_g is the heat generation rate of the chip, $\rho = \rho_{\text{ref}} = 978$ kg/m^3 and $c = c_{\text{ref}} = 4187$ J/(kg K) are respectively density and specific heat, which are kept constant in this study.

3. Cooling devices and computational domains

3.1. Fractal-channels

The first configuration of fractal channel considered in this study is the classical fractal-shaped network reported in figure 1 (Case A). Geometry is fully described by the number of bifurcations n, length L_0 and hydraulic diameter d_0 of the first branch, and the ratio between lengths and hydraulic diameters of two consecutive branches, respectively $\theta = L_{k+1}/L_k = N^{-1/\eta}$ and $\gamma = d_{k+1}/d_k = N^{-1/\psi}$. Geometric dimensions introduced are illustrated in figure 2. Channels of rectangular cross-section with uniform depth of $0.501\, l_{\text{ref}}$ are selected for manufacturing reasons, see for example refs. [1], [11] and [12]. Values of θ and γ are related to the parameters η and ψ. in Ref. [13] and [14] values $\eta = 3$ and $\psi = 3$ are recommended for reducing pressure drop. In this study it has been possible to set $\psi = 3$ while, due to the size of the chip selected $\eta = 3$ would cause channels to overlap. The channel lengths have been instead selected in order to fill the chip plan area with flow passages. Table 1 summarizes the geometric parameters of the first configuration studied.

The computational domain, depicted in figure 3, includes a single chip, which acts as the volumetric heat source, an aluminium plate, where the coolant passages are manufactured, the heat exchanger passages and the fluid flowing within the passages. An imposed mass flow rate of $0.010\, \rho_{\text{ref}}\, u_{\text{ref}}\, l_{\text{ref}}^2$ enters the domain from the side of the aluminium region at the constant temperature of $26.5\, T_{\text{ref}}$; it passes through the channels and at the highest fractal branch, it is

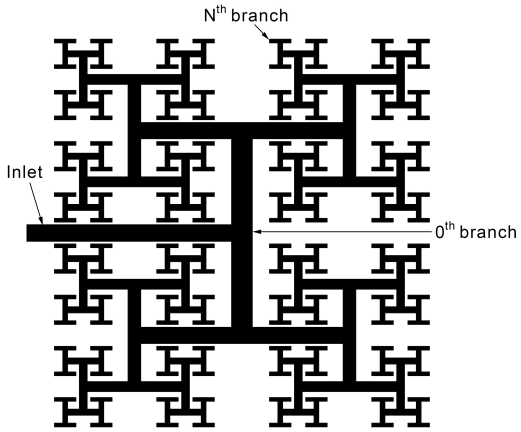

Figure 1. Fractal network.

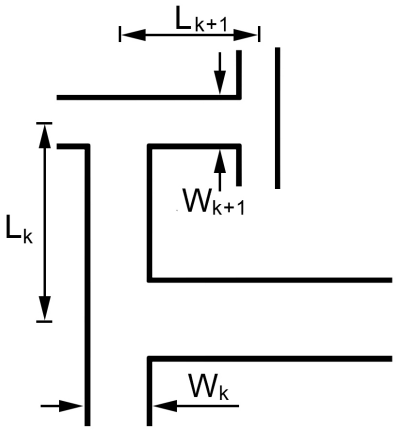

Figure 2. Fractal characteristic dimensions.

Table 1. Fractal-channel dimensions of the k-th level, Case A. Lengths are made non-dimensional using l_{ref}, defined as in equation (4).

k	H_k	W_k	L_k	d_k	L_k/d_k
Inlet	0.501	0.040	0.488	0.076	6.4
0	0.501	0.050	0.244	0.094	2.6
1	0.501	0.039	0.244	0.075	3.3
2	0.501	0.031	0.122	0.059	2.1
3	0.501	0.024	0.122	0.047	2.6
4	0.501	0.019	0.061	0.037	1.6
5	0.501	0.015	0.043	0.030	1.5
6	0.501	0.012	0.031	0.023	1.3
7	0.501	0.009	0.026	0.019	1.4

discharged into a plenum through rectangular holes. The fluid exits from the domain at the sides of this plenum at a given pressure.

At the top of the computational domain, which is the upper boundary of the discharge plenum, symmetry conditions are applied in order to set the first-order normal derivatives to zero and to reduce the influence of boundaries to the solution. The outlet pressure is fixed and homogeneous Neumann conditions are specified for each velocity component and temperature fields.

For the thermal field, lateral domain boundaries are adiabatic and heat is therefore extracted from the domain only through the liquid coolant. Since the geometry and fluid dynamics conditions are symmetric about the longitudinal middle plane of the inlet channel, only half of the domain described is considered in the simulations, see figure 3.

The computational grid used in the fractal-channel simulations involves about 3.9 millions hexahedral cells and is topologically structured, both in the solid and fluid regions. At the fluid-solid interface the AMI interpolation implemented in OpenFOAM is used in order to reduce the number of control volumes in the aluminium region. The maximum interpolation error on the wall heat flux is of 0.14% . The average and maximum distances between wall and first computational point distance are $y^+ = 0.55$ and $y^+ = 4.4$ wall units. Accordingly, a Low-Reynolds approach is applied.

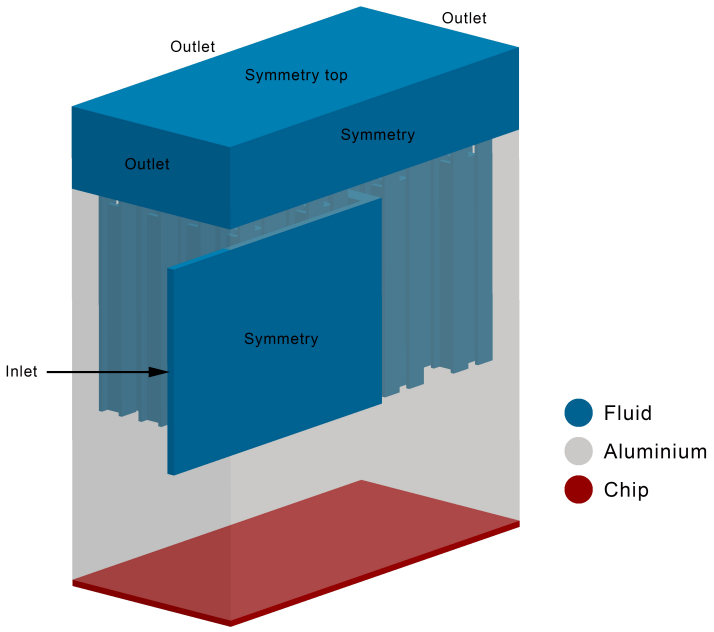

Figure 3. Computational domain and boundary conditions of the first fractal-channels configuration.

3.2. Submerged impinging jets

A second set of simulations has been performed on arrays of submerged impinging jets. Prior to the study of jet arrays, the accuracy of the numerical procedure has been checked by comparing results of two simulations of a single axisymmetric jet against experimental and numerical results, respectively published in Ref. [15] and [16]. Simulations are conducted resorting to an axisymmetric geometrical model. The jet diameter is 3.18 mm and a uniform heat flux of 25 W/cm^2 is imposed on the impingement plate; further details on the domain dimensions and boundary conditions can be found in Ref. [16]. Two turbulence models have been tested: the k-ε and the k-ω SST. In both cases the Low Reynolds approach is used for the near wall treatment, average and maximum distance of the first computational volumes from the wall are of $y^+ = 0.9$ and $y^+ = 2.9$ respectively. The comparison between present results and data from Ref. [15] and [16] is summarized in table 2. The radial profile of local heat transfer coefficient is reported in figure 4, where it appears that the k-ω SST model reproduces the experimental local heat transfer coefficient with a smaller error with respect to the k-ε model. Table 2 shows that also mass flow rate, reattachment point and discharge coefficient are predicted by the k-ω SST turbulence model more accurately. The discharge coefficient is computed as

$$c_D = \frac{\dot{m}_r}{\dot{m}_{id}} = \frac{4\ \dot{m}_r}{N\pi D^2\sqrt{2\,\rho\Delta p}} \tag{8}$$

where pressure losses are assumed lumped in the nozzle. In equation (8) $\dot{m}_r$ is the real mass flow rate, N and D are the number of jets and their diameter, Δp is the imposed pressure drop between inlet and outlet and ρ is the fluid density. As a consequence of this validation procedure the k-ω SST model is used in all the simulations of submerged impinging jets presented here.

The study of the jet array cooling strategy has been conducted performing several simulations varying the number of jets, their diameter and the aspect ratio(AR $= D/\delta$, where δ and D are the nozzle height and diameter), also by taking into account results reported in refs. [17], [18], [15],

Table 2. Comparison between present results, using k-ε and k-ω SST turbulence model, and data from papers [15] and [16]. In the table D is the nozzle diameter.

	k-ε	k-ω SST	Experiment [15]	Simulation [16]
Pressure drop (Pa)	7116	7116	7116	7250
Mass flow rate (kg/s)	0.0288	0.0310	0.0326	0.0326
Discharge coefficient	0.713	0.768	0.806	-
Reattachment length	-	$0.92D$	-	$0.80D$

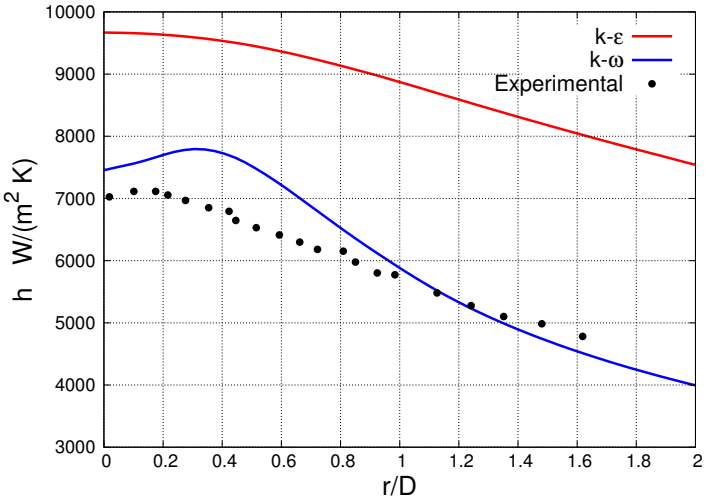

Figure 4. Radial profiles of local heat transfer coefficient in the single axisymmetric jet simulation: comparison between present results and experimental data [15].

[19], [20] and [21]. Among all the simulations performed, two configurations arise for thermal and fluid dynamics performance: arrays of 6×6 and 7×7 jets, with jets of diameter $0.050\, l_{\text{ref}}$, unit aspect ratio (AR = 1) and a distance between the nozzle plate and the impingement plate of $Z/D = 3$. In the following text, only these two cases are presented. Since the configuration is symmetric with respect to two orthogonal directions, the computational domain considers only a quarter of the full system. Configurations considered are shown in figure 5. The simulated domain is depicted in figure 6 and it involves a stack of different regions: a chip (which is the heat source), two layers of copper and ceramic, an aluminium plate and the coolant region, which include an inlet plenum, the nozzles and a discharge zone. The copper, ceramic and aluminium layers introduce a conductive thermal resistance for the heat flux per unit area of $60.2\, T_{\text{ref}}\, l_{\text{ref}}^2/P_{\text{ref}}$, $261.7\, T_{\text{ref}}\, l_{\text{ref}}^2/P_{\text{ref}}$ and $1105.9\, T_{\text{ref}}\, l_{\text{ref}}^2/P_{\text{ref}}$ respectively.

The coolant enters the domain by the lateral boundaries of the inlet plenum at a temperature of $60.9\, T_{\text{ref}}$, passes through the nozzles, exchanges heat from the aluminium plate and exits through the lateral boundaries in the discharge zone, see figure 6. The energy required for the fluid flow is provided by imposing a relative pressure of Δp_{ref} at the inlet and ambient pressure at the outlet. Symmetric boundary condition is imposed both at the top of the inlet plenum (for the same reasons provided for fractal channels, see section 3.1) and at the symmetry planes, while the no-slip condition is imposed at the other boundaries of the fluid region. The thermal input of $3.952 \times 10^{-3}\, P_{\text{ref}}$ relative to the entire chip is provided by setting a volumetric heat

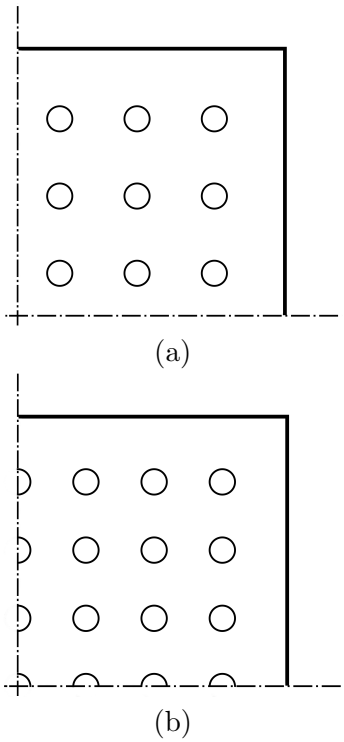

Figure 5. Nozzles arrangement: (a) 6×6 array, (b) 7×7 array.

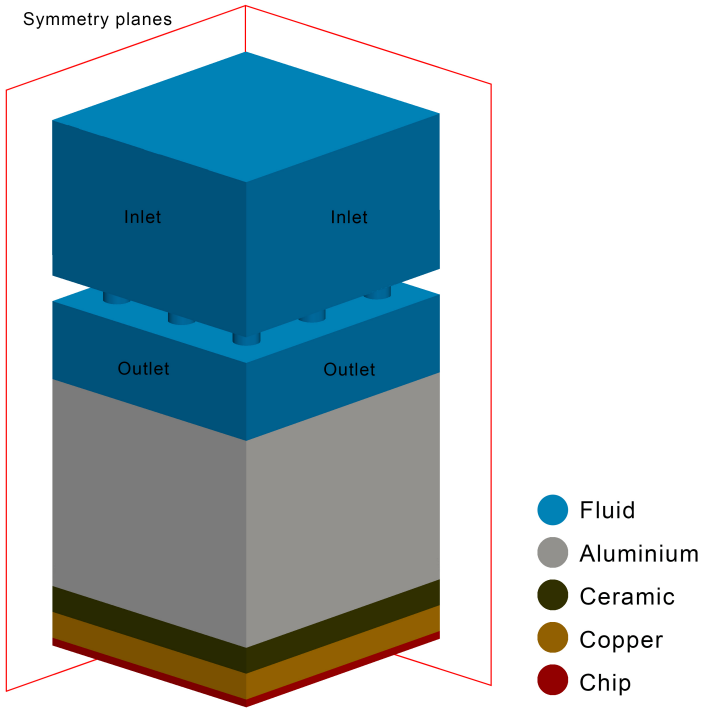

Figure 6. Computational domain of the 6×6 array configuration.

source in the chip, then heat is transferred in the vertical direction through the solid regions, and finally to the coolant. Lateral boundaries of the solid regions are set to adiabatic or symmetric, which at second order accuracy corresponds to the adiabatic condition.

The computational domain is discretised with about 2 million hexahedral cells and is topologically structured in both configurations. At the solid-fluid interface the mesh is conformal, thus no interpolation is applied. Since the computational grid allows to achieve y^+ average values of 0.92 and 0.88 for the 6×6 and 7×7 configuration respectively, the low Reynolds near wall treatment is imposed on the impingement plate in both cases.

4. Results

4.1. Fractal-channels

Figure 7(a) shows the temperature field on a section parallel to the chip, at the mid channel depth for case A. As expected, the temperature of the coolant increases but far enough from the inlet the fluid temperature is higher than the solid wall. The extent of this phenomenon is made clear in figure 7(b), in which the black line represents the perimeter of the solid-liquid interface where the solid walls are cooled, the red line indicates the portion of interface where the solid walls are heated. At the mid channel depth, the three last fractal levels are mostly characterized by inverse heat transfer and give place to an idle heat transfer loop.

Figures 8(a) and 8(b) reveal that the largest pressure drop is in the fluid discharge to the outlet plenum. No cooling effect is brought by this highly dissipative jet flow and mechanical energy is wasted in the discharge. A second region of remarkable pressure drop is in the first, largest branch.

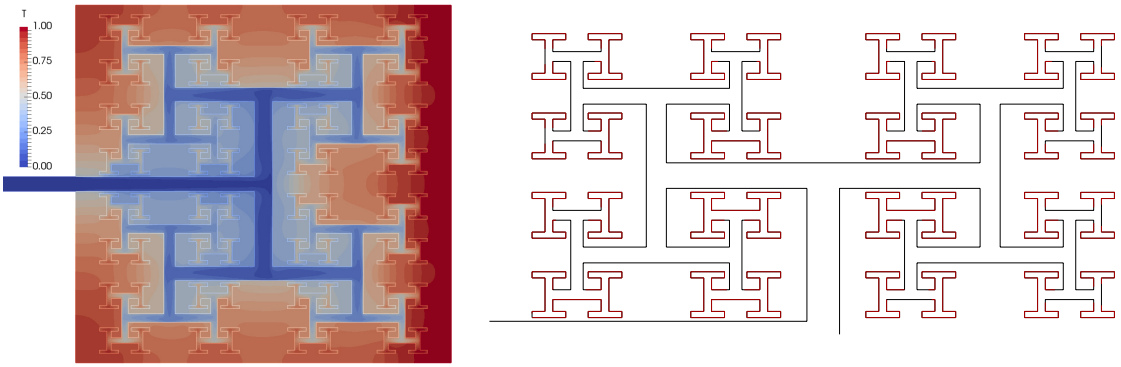

(a) (b)

Figure 7. (a) Temperature field on a section parallel to the chip at mid channel depth, in both aluminium and fluid regions, and (b) perimeter of the solid-fluid interface coloured according to the direction of heat transfer: black from solid to fluid, red from fluid to solid.

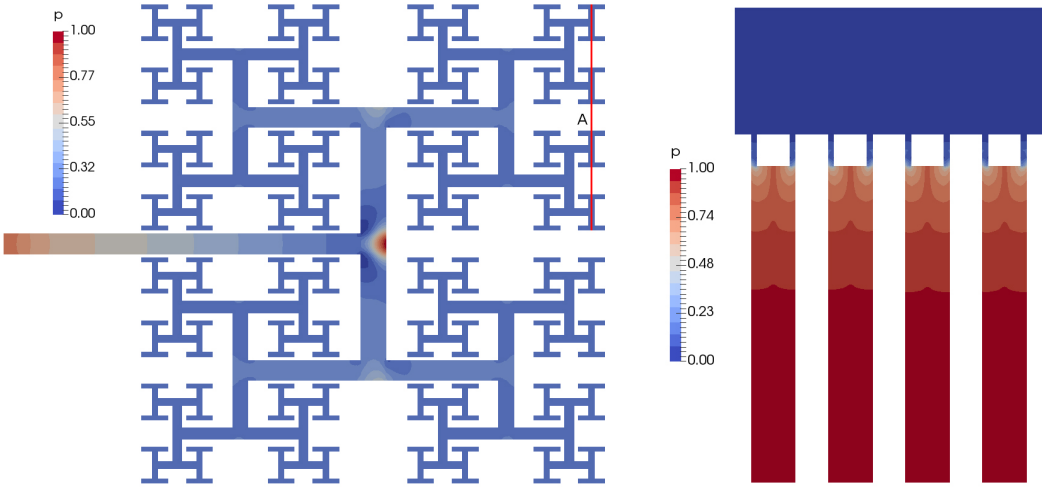

(a) (b)

Figure 8. Pressure field on a section parallel to the chip at mid channel depth (a), and on the section indicated by the red line (b).

Global results are summarized in table 3. The main disadvantage of this solution is in the large portion of wet area which exhibits negative heat transfer ($A_{w,h<0}$): it includes almost half the total wet area in the conditions set for this study. The amount of heat per unit time transferred back from the coolant to the aluminium region, $\dot{Q}_{\text{inv}}$ is more than one fourth of the heat input rate, and an idle heat transfer loop is formed. In summary this fractal-channel configuration allows to achieve a relatively low maximum temperature of the chip but the cost in terms of pumping power is high.

Results obtained in Case A suggested a set of geometrical modifications and the design of a potentially more efficient fractal-channel configuration (Case B). Geometrical modifications are listed below:

- removal of the two highest fractal levels;
- increased hydraulic diameter of the first branch;
- increased hydraulic diameter of the last branches;

Table 3. Overall performance of fractal-channels, Case A. Thermal resistance is made dimensionless by $T_{\text{ref}}/P_{\text{ref}}$, heat transfer coefficient by $P_{\text{ref}}/\left(l_{\text{ref}}^2 T_{\text{ref}}\right)$ and power by P_{ref}.

R_{th}	$\overline{h}$	P_{p}	$A_{w,h<0}$ (%)	$\dot{Q}_{\text{inv}}$ (%)
28401	$1.23{\cdot}10^{-5}$	$1.61{\cdot}10^{-8}$	49.7	27.3

Table 4. Fractal-channels dimensions in the enhanced configuration (Case B). Lengths are made non-dimensional using l_{ref}, defined as in equation (4).

k	H_k	W_k	L_k	d_k	L_k/d_k
Inlet	0.501	0.080	0.488	0.145	3.4
0	0.501	0.062	0.244	0.114	2.1
1	0.501	0.048	0.244	0.090	2.7
2	0.501	0.037	0.134	0.071	1.9
3	0.501	0.029	0.127	0.056	2.3
4	0.501	0.023	0.064	0.044	1.4
5	0.501	0.036	0.064	0.068	0.9

Table 5. Overall performance of the enhanced fractal-channels configuration. Thermal resistance is made dimensionless by $T_{\text{ref}}/P_{\text{ref}}$, heat transfer coefficient by $P_{\text{ref}}/\left(l_{\text{ref}}^2 T_{\text{ref}}\right)$ and power by P_{ref}.

R_{th}	$\overline{h}$	P_{p}	$A_{w,h<0}$ (%)	Q_{inv} (%)
3528	$1.75{\cdot}10^{-4}$	$3.06{\cdot}10^{-8}$	29.3	11.8

- reduction of the dimensions of channels close to the entrance duct.

Geometrical modifications applied are motivated also by the temperature field of figure 7(a), where a cold region close to the entrance duct is observed due to its proximity to the cold fluid.

The dimensions of Case B configuration are summarized in table 4. As reported in table 5, Case B configuration requires a much smaller pumping power, while the maximum temperature of the chip is not very different from Case A. Also in this second configuration about one third of the wet surface is characterized by an inverse heat flux. To overcome the inverse heat flux problem while keeping the same thermo-physical properties of the coolant, the volumetric flow rate should be substantially increased. Since the pressure drop required by fractal channel is already very high this solution is to be disregarded. The fractal channel configuration selected (Case A) and also its geometrically improved version (Case B) need to undergo a optimization procedure before being conveniently employed for the electronic cooling.

4.2. Submerged impinging jets

Contours of heat transfer coefficient on the aluminium plate are reported in figure 9. Note that this images are obtained mirroring the computational region about the symmetry planes. It is observed that jets interact, as shown by the different shapes of the high heat transfer coefficient

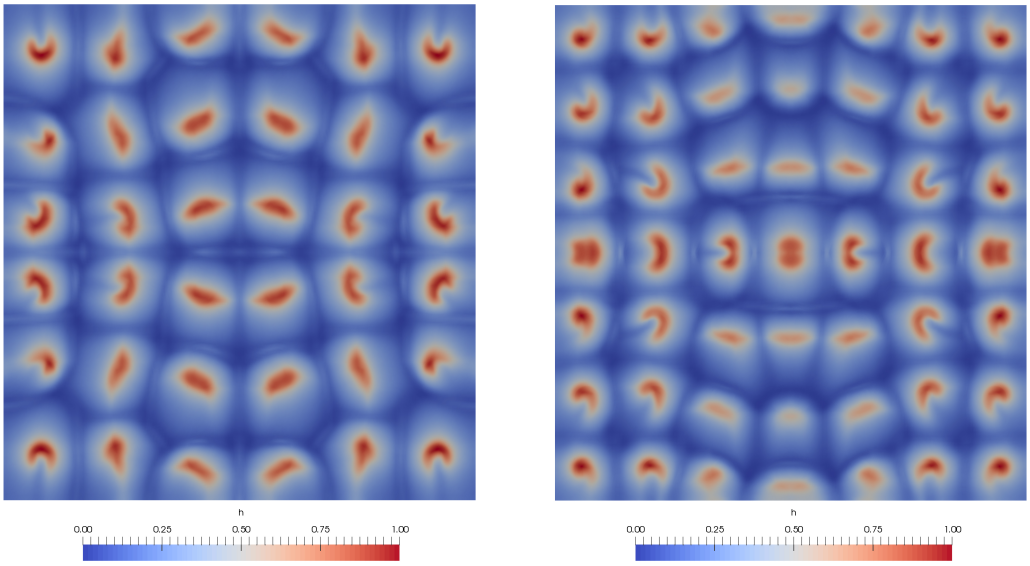

(a) (b)

Figure 9. Normalized heat transfer coefficient on the impingement plate: (a) 6×6 array, (b) 7×7 array.

Table 6. Comparison between overall results of the 6×6 and 7×7 array configurations.

Parameter	6×6	7×7
R_{th} $(\cdot\, T_{\text{ref}}/P_{\text{ref}})$	$3.73 \cdot 10^{3}$	$4.94 \cdot 10^{3}$
P_{p} $(\cdot\, P_{\text{ref}})$	$8.87 \cdot 10^{-8}$	$1.09 \cdot 10^{-7}$
$\overline{h}$ $(\cdot P_{\text{ref}}/\left(l_{\text{ref}}^2 T_{\text{ref}}\right))$	$4.49 \cdot 10^{-4}$	$3.45 \cdot 10^{-4}$
c_{D}	0.63	0.57

spots corresponding to each jet. The horizontal flow toward outlet deviates the jets, preventing the undisturbed impingement of every jets.

The overall performance of these configurations are summarized in table 6. Comparing solutions at constant pressure drop, the 7×7 array keeps the chip at almost 2 °C cooler than the 6×6 array, but the cost in terms of pumping power is 20% higher. The choice between these configurations depends upon the cooling system characteristics.

5. Discussion

The four cases considered are characterized by

- equal inlet temperature
- equal heat transfer rate

and following the reasoning in "Performance evaluation criteria for use of enhanced heat transfer surfaces in heat exchanger design" by Webb [22] the efficiency of each of the four configurations investigated can be assessed by comparison of the pumping power. It appears in table 7 where the ratios between dimensional pumping power required by fractal channels and by the two jet

Table 7. Comparison of pumping power required, thermal resistance and space averaged heat transfer coefficient. Numbers are obtained by division of the dimensional results by the smallest value. Subscripts A, B and refers to the case A and B respectively.

Parameter	Case A	Case B	6×6	7×7
$R_{\mathrm{th}}/R_{\mathrm{th,B}}$	1.00	1	1.68	1.64
$\overline{h}/\overline{h}_{\mathrm{A}}$	1	1.77	2.86	2.99
$P_{\mathrm{p}}/P_{\mathrm{p,6x6}}$	5.31	1.26	1	1.23

configurations are reported, that the 6×6 jet configurations exchange the same heat at the lowest cost in terms of mechanical power required.

On the other side, from the point of view of maximum temperature of the chip, fractal channels ensure a lower temperature, despite the occurrence of negative heat fluxes. This is clearly shown in table 7, where the ratios between dimensional thermal resistance of impinging jets and fractal channels are reported. Given the definition of thermal resistance of a heat exchanger, see equation (2), and the circumstance that heat transfer rate and inlet temperature of the coolant is equal in all cases R_{th} provides a measure of the maximum temperature of the cooled electronic device.

Fractal channels For fractal channels exchanging heat through only a small part of the wet surface, it can be demonstrated that aside from the pumping power required, heat transfer enhancement which is expected to derive from the large heat transfer surface of the highest fractal levels, is at best very small. Let us consider the ratio between heat transfer rate per unit length of two channels of diameter d_{k+1} (smaller diameter) with respect to a single channel of hydraulic diameter d_k (larger diameter) carrying the same volumetric flow rate of the coolant. This ratio represents heat transfer enhancement to be ascribed to heat transfer surface increase.

Considering the canonical form of the Nusselt number dependence upon Re which applies to fully developed flow in pipes,

$$\mathrm{Nu} = \zeta \, \mathrm{Re}^{\alpha} \, \mathrm{Pr}^{\beta} \tag{9}$$

and Dittus-Boelter correlation which is reported to be valid for liquids in turbulent flow regime $\mathrm{Re} > 10^4$ prescribes $\alpha = 4/5$ while for a given fluid in laminar conditions $\alpha = 0$

$$\frac{\dot{Q}_{k+1}}{\dot{Q}_k} = \left(\frac{\mathrm{Re}_{k+1}}{\mathrm{Re}_k} \right)^{\alpha} \frac{d_k}{d_{k+1}} \frac{2\, M_{k+1}}{M_k} \frac{\Delta T_{k+1}}{\Delta T_k} \tag{10}$$

where M_k indicates wet surface at fractal level k, and leads to

$$\frac{\dot{Q}_{k+1}}{\dot{Q}_k} = \left(\frac{2M_{k+1}}{M_k} \right)^{(1-\alpha)} \frac{d_k}{d_{k+1}} \frac{\Delta T_{k+1}}{\Delta T_k} \tag{11}$$

For self-similar cross sections where $M_k/d_k = M_{k+1}/d_{k+1}$

$$\frac{\dot{Q}_{k+1}}{\dot{Q}_k} = 2^{(1-\alpha)} \left(\frac{M_k}{M_{k+1}} \right)^{\alpha} \frac{\Delta T_{k+1}}{\Delta T_k} \tag{12}$$

and for laminar flow ($\alpha = 0$)

$$\frac{\dot{Q}_{k+1}}{\dot{Q}_k} = 2 \, \frac{\Delta T_{k+1}}{\Delta T_k} \tag{13}$$

raising fractal level can increase heat transfer rate, provided temperature differences at subsequent time levels do not decrease too fast.

Let us consider coefficient C_{k+1}, defined as

$$C_{k+1} \equiv \frac{\dot{Q}_{k+1}}{\dot{Q}_k} \frac{\Delta T_k}{\Delta T_{k+1}} \tag{14}$$

so that for $C_{k+1} > 1$ heat transfer augmentation is expected. In the present case, a series of channels of rectangular cross section is considered of sides W_k and H, where $W_k < H$. In case $W_{k+1} = W_k/2$ and $H = \Gamma_{k+1} H_{k+1}$

$$C_{\mathrm{k+1}} = \left(\frac{2 + 2\Gamma_{k+1}}{2 + \Gamma_{k+1}} \right)^{(2-\alpha)} \tag{15}$$

which for $\Gamma_{k+1} > 0$ is a increasing function of Γ_{k+1} tending to $2^{(2-\alpha)}$ for elongated rectangles (large Γ_{k+1}).

In fractal channel applications it might occur that not all the wet surface is involved in the heat transfer. In case just one of the small sides W_k contributes to heat transfer the heat augmentation coefficient in turbulent flow conditions is given by

$$C_{\mathrm{k+1}} = \left(\frac{2 + 2\Gamma_{k+1}}{2 + \Gamma_{k+1}} \right)^{(1-\alpha)} \tag{16}$$

Coefficient C_{k+1} increases with Γ_{k+1} tends to $2^{(1-\alpha)}$ for elongated channels which equals $2^{(1-\alpha)} \approx 1.15$ in turbulent conditions. In laminar conditions

$$C_{\mathrm{k+1}} = \frac{2 + 2\Gamma_{k+1}}{2 + \Gamma_{k+1}} \tag{17}$$

tends to 2 for elongated channels. We have shown that heat transfer augmentation of fractal channels, whose favourable heat transfer features are expected to descend from the large heat transfer surface of the highest fractal levels, is only marginal.

6. Conclusions

Simulation results show that before fractal channels can be employed for electronics cooling applications their geometry need to undergo a multi-objective optimization procedure, which would probably modify their canonical shape and geometry.

Results reported suggest that the space averaged temperature difference between solid wall and fluid is too small, the difference becomes negative over a considerable portion of the fluid-solid interface, giving place to an idle heat transfer loop. In view of improving performances while keeping the same thermo-physical characteristics of the liquid, an increase in the coolant mass flow rate might be tried but the pumping power required for circulation is already too large, for example with respect to the submerged impinging jet solution.

Aside from the pumping power required, it is demonstrated in the text that when fractal channels are used for exchanging heat, these can be conveniently applied only in the case of heat transferred trough the whole channel wet surface.

As soon as a small part of the wet surface is used for heat transfer, a raise in fractal level is demonstrably characterized by a heat transfer augmentation which is at best very limited because the main heat transfer enhancement mechanism of fractal channels is almost neutralized.

Considering also the temperature difference between fluid and solid, it can be concluded that fractal channels are not conveniently applied in the cooling of flat, solid plates, *e.g.* for electronics cooling.

On the other side, heat transfer studies on arrays of submerged impinging jets under very similar conditions as the fractal channels show that these jets can exchange heat at a low cost in terms of mechanical pumping power. Their space-averaged overall heat transfer coefficient is very large. The few drawbacks affecting this solution include the temperature of the chips, which is in our case slightly higher than for fractal channels and the observation that, given the small nozzle diameters, impinging jets might be prone to fouling and obstruction and very sensitive to construction tolerances. Impinging jets are instead very flexible in terms of geometry, because the distribution of orifices can be specifically designed to specifically cool regions generating heat at high rates.

References

[1] Chen Y and Cheng P 2002 *Int. J. Heat and Mass Transf.* **45** 2643–48
[2] Senn S M and Poulikakos D 2004 *J. Power Sources* **130** 178–191
[3] Wang X-Q, Mujumdar A S and Yap C 2006 *Int. J. Thermal Sciences* **45** 1103–1112
[4] Escher W, Michel B and Poulikakos D 2009 *Int. J. Heat and Mass Transf.* **52** 1421–1430
[5] Jörg J, Taraborrelli S, Sarriegui S, De Doncker R W, Kneer R and Rohlfs W 2018 *IEEE Trans. Power Electron.* **33** 4224–4237
[6] Rau M J and Garimella S V 2013 *Int. J. Heat and Mass Transf.* **24** 715–726
[7] Penumadu P S and Rao A G 2017 *Appl. Therm. Eng.* **110** 1511–1524
[8] Menter F R, 1993 *AIAA Journal*, **32** 1598-1605.
[9] Ferziger J H and Perić M, 2002 *Computational Methods for Fluid Dynamics.*
[10] Tuckerman D B and Pease R F W 1981 *IEEE Elect. dev. letters* **2** 126–9.
[11] Hong F J, Cheng P, Ge H and Joo G T 2007 *Int. J. Heat and Mass Transf.* **50** 4986–98
[12] Chen Y, Zhang C, Shi M and Yang Y 2010 *AIChE J.* **56** 2018–29
[13] Bejan A and Errera M R 1997 *Fractals* **5** 685–95
[14] Murray C D 1926 *Proc. National Academy of Sciences* **12** 207–14
[15] Garimella S V and Rice R A 1995 *J. Heat Transfer* **117** 871–7
[16] Morris G K and Garimella S V 1998 *J. Elect. Packaging* **120** 68–72
[17] Garimella S V and Nenaydykh B 1995 *ASME-PUBLICATIONS-HTD* **319** 49–58
[18] Garimella S V and Nenaydykh B 1996 *Int. J. Heat and Mass Transf.* **39** 2915–23
[19] Li C and Garimella S V 2001 *Int. J. Heat and Mass Transf.* **44** 3471–80
[20] Robinson A J and Schnitzler E 2007 *Exp. Thermal and Fluid Sc.* **32** 1–13
[21] Whelan B P and Robinson A J 2009 *Appl. Therm. Eng.* **29** 11–2
[22] Webb R L 1981 *Int. J. Heat and Mass Transf.* **24** 715–726